Couple molecular excitons to surface plasmon polaritons in an organic-dye-doped nanostructured cavity

Kun Zhang, Wen-Bo Shi, Di Wang, Yue Xu, Ru-Wen Peng, Ren-Hao Fan, Qian-Jin Wang, and Mu Wang

Citation: Applied Physics Letters **108**, 193111 (2016); doi: 10.1063/1.4949562
View online: http://dx.doi.org/10.1063/1.4949562
View Table of Contents: http://scitation.aip.org/content/aip/journal/apl/108/19?ver=pdfcov
Published by the AIP Publishing

Couple molecular excitons to surface plasmon polaritons in an organic-dye-doped nanostructured cavity

Kun Zhang, Wen-Bo Shi, Di Wang, Yue Xu, Ru-Wen Peng,[a] Ren-Hao Fan, Qian-Jin Wang, and Mu Wang[a]
National Laboratory of Solid State Microstructures, School of Physics, and Collaborative Innovation Center of Advanced Microstructures, Nanjing University, Nanjing 210093, China

(Received 25 February 2016; accepted 3 May 2016; published online 13 May 2016)

In this work, we demonstrate experimentally the hybrid coupling among molecular excitons, surface plasmon polaritons (SPPs), and Fabry-Perot (FP) mode in a nanostructured cavity, where a J-aggregates doped PVA (polyvinyl alcohol) layer is inserted between a silver grating and a thick silver film. By tuning the thickness of the doped PVA layer, the FP cavity mode efficiently couples with the molecular excitons, forming two nearly dispersion-free modes. The dispersive SPPs interact with these two modes while increasing the incident angle, leading to the formation of three hybrid polariton bands. By retrieving the mixing fractions of the polariton band components from the measured angular reflection spectra, we find all these three bands result from the strong coupling among SPPs, FP mode, and excitons. This work may inspire related studies on hybrid light-matter interactions, and achieve potential applications on multimode polariton lasers and optical spectroscopy. *Published by AIP Publishing.* [http://dx.doi.org/10.1063/1.4949562]

Recently, controlling light-matter interactions by nanostructures[1–20] has attracted much attention, due to both fundamental and practical interest. Up to now, coupling between photons and excitons has been extensively studied by many groups, theoretically and experimentally, ranging from weak coupling regime[1,2] to strong coupling regime[1,3–13] and even ultrastrong coupling regime.[14–19] In the weak coupling regime, the damping rates of the photons and excitons prevails over the energy exchange rate between them, and the line shapes of the absorption or emission are modified. This may have promising applications in the areas of solar cells and sensors. On the other hand, in the strong and ultrastrong coupling regimes where the energy exchange rate prevails over their damping rates, hybrid optical modes with light-like and matter-like components generate. In other words, strong coupling leads to the formation of quasi-particles named polaritons, with small mass and easy to be optically controlled, which can be used to explore some fundamental problems, such as Bose-Einstein condensation[21–23] and superfluid related phenomena.[24–26] Also, it inspires the design of polariton nanolasers.[27–29] What's more, it offers possibilities to realize all-optical circuits[30] and photonic quantum devices.[31]

There are various systems used to study strong coupling, such as optical microcavities,[3–5,9,32] multilayered distributed Bragg reflector (DBR),[7,21–25] and metallic nanostructures.[8,10–13,33] These systems offer diverse platforms supporting cavity modes or surface plasmon polaritons (SPPs), which can guide and manipulate light at nanoscale dimensions. Meanwhile, semiconductor nanostructures and some organic dyes inserted in these systems can offer excitons to interact with light. In the previous work, some systems supporting hybrid modes have also been reported.[34–36] In these systems, one cavity mode can couple with two kinds of excitons,[34] one kind of excitons can couple with a series of cavity modes,[35] or two kinds of plasmons can couple with the same kind of excitons.[36] Such hybrid systems introduce interesting properties to strong coupling, such as tunability and integration, extending their applications. Here, we offer another choice to realize hybrid light-matter interactions, simultaneously involving the interactions among SPPs, Fabry-Perot (FP) cavity mode, and molecular excitons. We design the organic-dye doped nanostructure by the simulation software, and experimentally demonstrate the hybrid strong coupling, which leads to three hybrid polariton bands. Afterwards, we retrieve from the experimental data to get the mixing fractions of SPPs, FP cavity mode, and excitons in these hybrid bands, which helps to verify the origin of the three bands. Our system involves two kinds of light components to form hybrid polaritons, one with strong dispersion (i.e., SPPs) and the other one nearly nondispersion (i.e., FP mode), which may inspire related studies about hybrid light-matter interactions and achieve potential applications on multimode polariton lasers and optical spectroscopy.

We first consider a nanostructure with PVA (polyvinyl alcohol), which is an ordinary dielectric layer, inserted between a silver grating and a thick silver film, as illustrated in the inset of Figure 1(a). The grating is used to introduce SPPs,[37–39] and the inserted PVA layer helps to form a Fabry-Perot (FP) cavity[40] between the grating and the silver layer. The period of the grating can be changed to tune the SPPs energy, and the thickness of the PVA layer can be changed to tune the FP mode energy. We design our grating with a 300 nm period and a 40 nm slit width. The thickness of the PVA layer is 170 nm. Figure 1(a) shows the reflection spectrum calculated by the commercial finite-difference time-domain (FDTD) simulation software package (Lumerical FDTD Solutions). There are two reflection dips, corresponding with two modes in this nanostructure. In order to explore the origin and the feature of these modes, we monitor the

[a]Authors to whom correspondence should be addressed. Electronic addresses: rwpeng@nju.edu.cn and muwang@nju.edu.cn

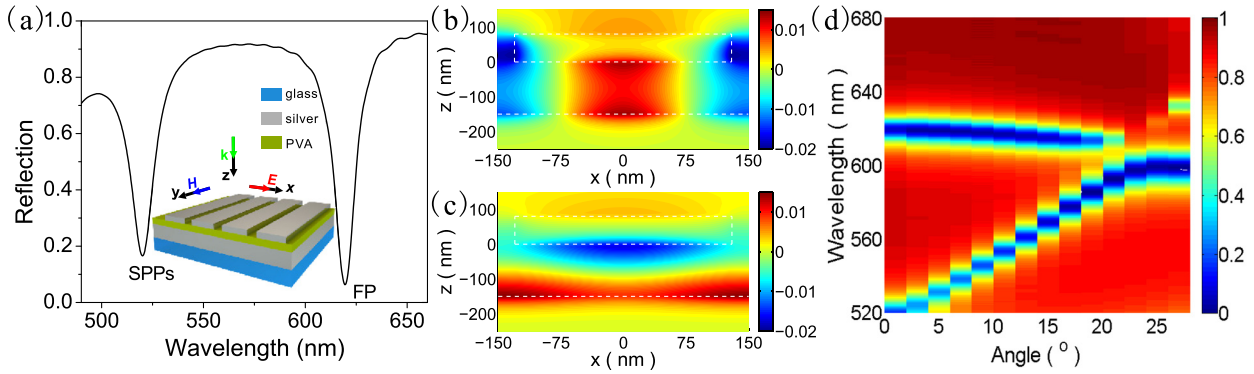

FIG. 1. (a) The calculated reflection spectrum of the nanostructure with PVA inserted between a silver grating and a thick silver film. The inset gives a schematic description of the nanostructure. The field distribution of H_y in the x-z plane (b) at the wavelength marked as SPPs and (c) at the wavelength marked as FP. (d) The two-dimensional map of calculated reflection spectra under different incident angles.

distributions of the magnetic field component H_y in the x-z plane at the two dips, as shown in Figs. 1(b) and 1(c), and also calculate the reflection spectra under different incident angles, as mapped in Fig. 1(d). Using the method in Ref. 32, we find that the first dip around 520 nm results from the SPPs induced by the grating, which have strong dispersion. On the other hand, the second one around 620 nm is almost nondispersive. And in simulation, we find that this mode shifts to longer wavelength as the thickness of PVA increasing, together with the field distribution, both indicating an FP mode. Moreover, when the incident angle is around 20°, the SPPs mode strongly couples with the FP mode, resulting in the anti-crossing in Fig. 1(d). Although the field distributions at these two dips look different, the light is strongly trapped in the PVA layer for both modes, offering the possibility of strong coupling.

We then replace the pure PVA layer with the J-aggregates doped PVA layer, in order to introduce excitons, as sketched in Figure 2(a). The used cyanine dye is TDBC (5,6-Dichloro-2-[[5,6-dichloro-1-ethyl-3-(4-sulfobutyl)-benzimidazol-2-ylidene]-propenyl]-1-ethyl-3-(4-sulfobutyl)-benzimidazolium hydroxide, inner salt, sodium salt), whose chemical formula is given in the inset of Fig. 2(a). The experimentally measured absorption spectrum and normalized photoluminescence (PL) spectrum of the formed J-aggregates are both given in Fig. 2(b), indicating the exciton energy to be 2.11 eV (around 589 nm). This energy is close to the FP mode energy, so there could be an effective coupling between the FP mode and the molecular excitons. Here, we can reasonably treat the FP mode in this system as nearly dispersion-free mode. In this way, the interaction can be described by the coupled equations as follows:

$$\begin{pmatrix} E_{fp} & \hbar\Omega/2 \\ \hbar\Omega/2 & E_{ex} \end{pmatrix} \begin{pmatrix} \alpha_{fp} \\ \alpha_{ex} \end{pmatrix} = E_i \begin{pmatrix} \alpha_{fp} \\ \alpha_{ex} \end{pmatrix}, \tag{1}$$

where E_{fp} and E_{ex} are the energies of FP mode and excitons, $\hbar\Omega$ is the coupling energy between the FP mode and

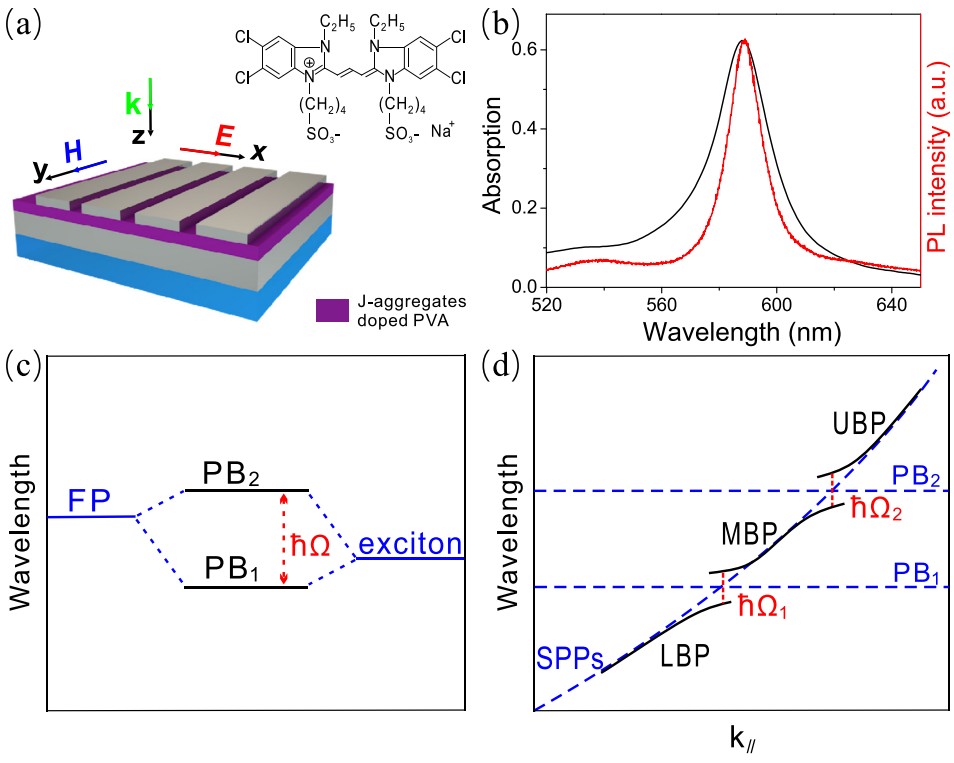

FIG. 2. (a) A schematic description of the J-aggregates doped nanostructure. And the inset shows the chemical formula of the TDBC used to form J-aggregates. (b) The measured absorption spectrum (black line) and the normalized photoluminescence (PL) spectrum (red line) of the J-aggregates. (c) Sketch of the interaction between J-aggregates excitons and FP mode. (d) Sketch of the interactions among SPPs mode, PB_1 mode, and PB_2 mode.

excitons, E_i is the energy of the hybrid mode, and the mixing fractions $|\alpha_{fp}|^2$ and $|\alpha_{ex}|^2$ represent the relative weightings of FP mode and excitons in the hybrid mode. There are two unique solutions for E_i and thus there are two hybrid modes emerging. Owing to the nearly nondispersion of the FP mode and the nondispersion of the excitons, these hybrid modes almost do not disperse with the in-plane wave vector. As schematically shown in Fig. 2(c), we label these two modes as PB_1 and PB_2.

However, as the SPPs mode has a strong dispersion, it would interact with the PB_1 and PB_2 modes successively while we change the incident angles. Consequently, there would be hybrid dispersive polariton bands. This hybrid coupling can be approximately described by the coupled oscillator model, expressed as

$$\begin{pmatrix} E_{sp} & \hbar\Omega_1/2 & \hbar\Omega_2/2 \\ \hbar\Omega_1/2 & E_1 & 0 \\ \hbar\Omega_2/2 & 0 & E_2 \end{pmatrix} \begin{pmatrix} \alpha_{sp} \\ \alpha_1 \\ \alpha_2 \end{pmatrix} = E_p(\theta) \begin{pmatrix} \alpha_{sp} \\ \alpha_1 \\ \alpha_2 \end{pmatrix}, \quad (2)$$

where E_{sp}, E_1, and E_2 are the energies of SPPs mode, PB_1 mode, and PB_2 mode, $\hbar\Omega_1$ or $\hbar\Omega_2$ is the coupling energy between SPPs mode and PB_1 or PB_2 mode, $E_p(\theta)$ represents the dispersive energy of the hybrid polariton band, and the mixing fractions $|\alpha_{sp}|^2$, $|\alpha_1|^2$, and $|\alpha_2|^2$ are the relative weightings of SPPs mode, PB_1 mode, and PB_2 mode in the polariton band. There are three unique solutions for $E_p(\theta)$, which means we can finally get three dispersive polariton bands in this nanostructure. We name these hybrid polariton bands as lower polariton band (LPB), middle polariton band (MPB), and upper polariton band (UPB) to distinguish, as schematically described in Fig. 2(d).

To verify the prediction above, we fabricate the samples using the parameters used in simulation. After a 200 nm thick silver film is deposited onto the glass substrate via magnetron sputtering, a 170 nm J-aggregates doped PVA layer is spun onto it, and then an 80 nm silver film is deposited by magnetron sputtering. Finally, the gratings are fabricated on the top silver film by focus-ion-beam milling (FIB, Helios Nanolab 600i). Figure 3(a) shows the top view and side view scanning electronic microscope (SEM) image of the J-aggregates doped sample. We measure the reflection spectra of this sample under different incident angles and show some of them in Fig. 3(b). At normal incidence, we can clearly see three dips in the spectrum, corresponding with the three modes, i.e., SPPs mode around 518 nm, PB_1 mode around 578 nm, and PB_2 mode around 628 nm, respectively, as marked near the red line in Fig. 3(b). As the incident angle increases, the SPPs mode successively overlaps and couples strongly with the PB_1 and PB_2 modes, leading to the emergence of three hybrid polariton modes, tracked by the solid black lines in Fig. 3(b). We can see these hybrid modes more clearly from the two-dimensional map of the reflection spectra in Fig. 3(c), in which we fit the polariton bands by using Eq. (2), shown as black dashed lines. We can distinctly see three dispersive polariton bands in this map, and the calculated lines fit well with the experimental results. These polariton bands undergo anti-crossing at the points where the SPPs mode overlaps with PB_1 or PB_2 mode, with Rabi splitting energies of $\hbar\Omega_1 = 110.6$ meV and $\hbar\Omega_2 = 122.5$ meV, respectively, indicating the strong coupling between the SPPs mode and the PB_1 or PB_2 mode. This phenomenon matches well with the one predicted in Fig. 2(d).

Using the experimental data, we can retrieve the relative mixing fractions of SPPs mode, PB_1 mode, and PB_2 mode in the three polariton bands, i.e., $|\alpha_{sp}|^2$, $|\alpha_1|^2$, and $|\alpha_2|^2$, which are shown in Figs. 4(a)–4(c), respectively. As a matter of fact, these polariton bands originally come from the interactions among the three fundamental elements, SPPs, FP mode, and excitons. In this way, we finally get the mixing fractions of SPPs, FP mode, and excitons in these hybrid bands, and the results are given in Figs. 4(d)–4(f). In Fig. 4(a), we find the LPB mainly comes from the mixing of SPPs mode and PB_1 mode. Experimentally, the LPB approaches but never touches the PB_1 mode as the incident angle increasing (in Fig. 3(c)), agreed with the increase of PB_1 mode mixing fraction. But, in fact, LPB consists of three components as shown in Fig. 4(d). In our nanostructure, the wavelength of FP mode is longer than that of the excitons; therefore, although the mixing fractions of the FP mode and excitons both increase as the incident angle increasing, the mixing fraction of excitons eventually exceeds that of the FP mode at larger incident angles. In Figs. 4(b) and 4(e) for MPB, the mixing fraction of SPPs mode reaches the highest point at about 18°, matching well with the intersection point of SPPs mode and MPB as shown in Fig. 3(c). On the other hand, as the experimental data in Fig. 3(c) shows, MPB leaves PB_1 and approaches PB_2 with the incident angle increasing, leading to the decrease of

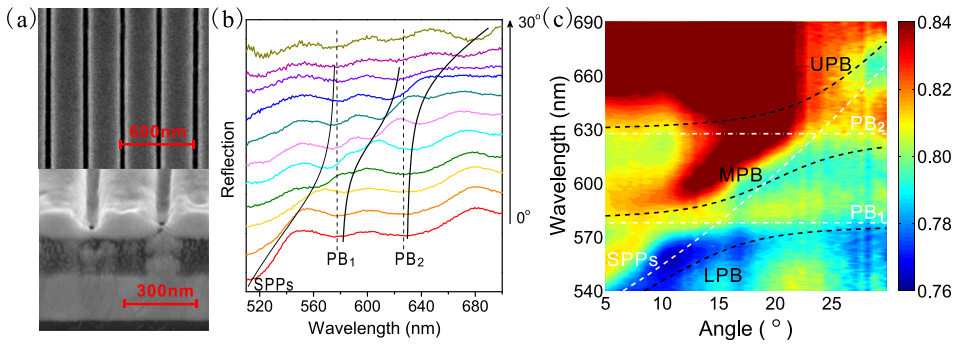

FIG. 3. (a) Top view and side view SEM images of the J-aggregates doped sample. (b) The reflection spectra of the sample under different incident angles. The solid black lines trace the three dispersive polariton bands, and the dotted black lines indicate the PB_1 mode and PB_2 mode. The SPPs mode under normal incidence is also indicated. (c) The two-dimensional map of the reflection spectra while scanning the incident angle. The white dashed line indicates the SPPs mode, the white dashed-and-dotted lines indicate the PB_1 and PB_2 modes, and the black dashed lines fit the three hybrid polariton modes.

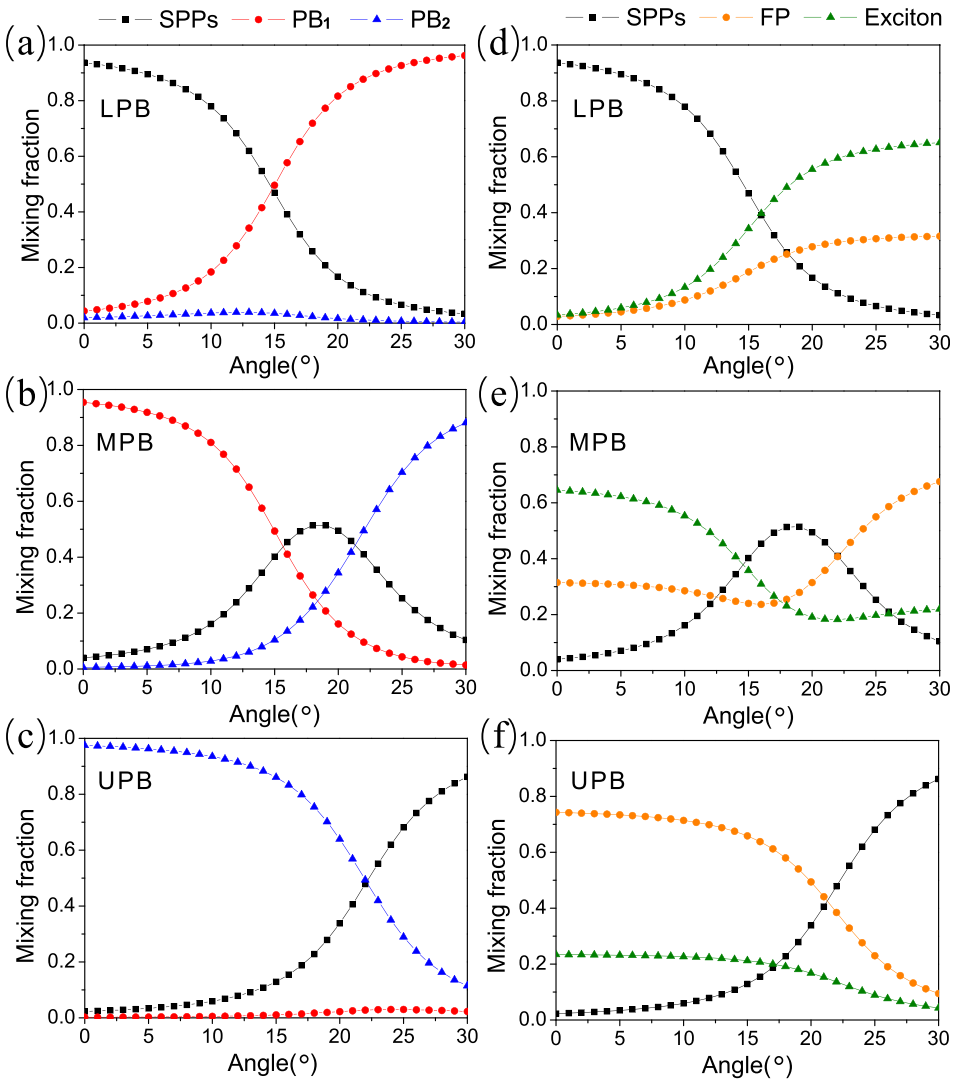

FIG. 4. The mixing fractions in the three modes, retrieved from the experimental data. (a)–(c)The mixing fractions of SPPs ($|\alpha_{sp}|^2$), PB_1 ($|\alpha_1|^2$), and PB_2 modes ($|\alpha_2|^2$). (d)–(f) The mixing fractions of SPPs, FP mode, and molecular excitons.

PB_1 mixing fraction and the increase of PB_2 mixing fraction (as shown in Fig. 4(b)). In fact, with the increase of incident angle, MPB goes across excitonic mode and FP mode successively, so in Fig. 4(e) we can find the mixing fraction of the excitons decreases and that of the FP mode increases. As UPB exists in the long wavelength region, it looks like that the UPB mainly comes from the interaction of SPPs and PB_2, as shown in Fig. 4(c). As the incident angle increases, the UPB leaves the PB_2 mode, resulting in the increase of SPPs mixing fraction and the decrease of PB_2 mixing fraction. Essentially, the UPB also comes from the interactions among the SPPs, FP mode, and excitons, as described in Fig. 4(f). Because UPB is closer to the FP mode rather than the excitons, the mixing fraction of FP mode is larger. But as the incident angle increases, UPB leaves the FP mode and excitonic mode, leading to the decrease of the two mixing fractions. In brief, although the dispersion features of the three polariton bands (LPB, MPB, and UPB) are different, these bands all originally result from the hybrid interactions among SPPs, FP mode, and excitons.

In our J-aggregates doped nanostructure, we simultaneously introduce SPPs, FP cavity mode, and molecular excitons. We tune the energy of SPPs and FP mode to make sure the three elements could efficiently couple with one another. Such hybrid interactions lead to three polariton bands and every hybrid band has three components. There are two kinds of light components in these finally formed polariton bands, which are SPPs with strong dispersion and the FP mode nearly dispersion-free, respectively. So every hybrid polariton band has strongly dispersive light component, nearly nondispersive light component and matter component. The only difference among the polariton bands is the different mixing fractions of the basic components, resulting in different dispersion features. What's more, as the energies of SPPs and FP mode can be easily tuned by the geometry parameters, our system can be used to offer hybrid interactions with different kinds of excitons. Such hybrid interactions may find interesting applications in multimode polariton lasers and quantum optics.

In summary, we have proposed and experimentally demonstrated an organic-dye-doped nanostructure to simultaneously introduce three fundamental elements, SPPs, FP cavity mode, and excitons, in which hybrid light-matter interactions take place. As a result, three hybrid polariton bands emerge. All these polariton bands are composed of the three basic components, i.e., SPPs with strongly dispersive photonic feature, FP mode with nearly nondispersive photonic feature, and molecular excitons acting as matter. By retrieving from the experimental data, we get the mixing fractions of SPPs, FP cavity mode, and excitons in these hybrid bands, finding

out the origin of the three bands. The experimental results match well with the theoretical prediction, and the retrieved data give a reasonable explanation of the experimental phenomenon. This work may inspire related studies about hybrid light-matter interactions and achieve some potential applications, such as plasmonic devices, multimode polariton lasers, and optical spectroscopy.

This work was supported by the Ministry of Science and Technology of China (Grant No. 2012CB921502), and the National Natural Science Foundation of China (Grant Nos. 61475070, 11474157, 11321063, 51302268, and 91321312).

[1]L. Shi, T. K. Hakala, H. T. Rekola, J. P. Martikainen, R. J. Moerland, and P. Törmä, Phys. Rev. Lett. **112**, 153002 (2014).
[2]S. Balci, E. Karademir, C. Kocabas, and A. Aydinli, Opt. Lett. **39**, 4994 (2014).
[3]J. Bellessa, C. Bonnand, and J. C. Plenet, Phys. Rev. Lett. **93**, 036404 (2004).
[4]S. Hayashi, Y. Ishigaki, and M. Fujii, Phys. Rev. B **86**, 045408 (2012).
[5]A. González-Tudela, P. A. Huidobro, L. Martín-Moreno, C. Tejedor, and F. J. García-Vidal, Phys. Rev. Lett. **110**, 126801 (2013).
[6]W. Wang, P. Vasa, R. Pomraenke, R. Vogelgesang, A. D. Sio, E. Sommer, M. Maiuri, C. Manzoni, G. Cerullo, and C. Lienau, ACS Nano **8**, 1056 (2014).
[7]S. Pirotta, M. Patrini, M. Liscidini, M. Galli, G. Dacarro, G. Canazza, G. Guizzetti, D. Comoretto, and D. Bajoni, Appl. Phys. Lett. **104**, 051111 (2014).
[8]E. Eizner and T. Ellenbogen, Appl. Phys. Lett. **104**, 223301 (2014).
[9]D. Ballarini, M. D. Giorgi, S. Gambino, G. Lerario, M. Mazzeo, A. Genco, G. Accorsi, C. Giansante, S. Colella, S. D'Agostino, P. Cazzato, D. Sanvitto, and G. Gigli, Adv. Opt. Mater. **2**, 1076 (2014).
[10]E. Karademir, S. Balci, C. Kocabas, and A. Aydinli, Opt. Express **22**, 21912 (2014).
[11]B. G. DeLacy, O. D. Miller, C. W. Hsu, Z. Zander, S. Lacey, R. Yagloski, A. W. Fountain, E. Valdes, E. Anquillare, M. Soljačić, S. G. Johnson, and J. D. Joannopoulos, Nano Lett. **15**, 2588 (2015).
[12]A. Benz, S. Campione, J. F. Klem, M. B. Sinclair, and I. Brener, Nano Lett. **15**, 1959 (2015).
[13]G. Zengin, M. Wersäll, S. Nilsson, T. J. Antosiewicz, M. Käll, and T. Shegai, Phys. Rev. Lett. **114**, 157401 (2015).
[14]Y. Todorov, A. M. Andrews, R. Colombelli, S. De Liberato, C. Ciuti, P. Klang, G. Strasser, and C. Sirtori, Phys. Rev. Lett. **105**, 196402 (2010).
[15]T. Schwartz, J. A. Hutchison, C. Genet, and T. W. Ebbesen, Phys. Rev. Lett. **106**, 196405 (2011).
[16]M. Geiser, F. Castellano, G. Scalari, M. Beck, L. Nevou, and J. Faist, Phys. Rev. Lett. **108**, 106402 (2012).
[17]S. Balci, C. Kocabas, B. Küçükö, A. Karatay, E. Akhüseyin, H. G. Yaglioglu, and A. Elmali, Appl. Phys. Lett. **105**, 051105 (2014).
[18]S. Gambino, M. Mazzeo, A. Genco, O. D. Stefano, S. Savasta, S. Patanè, D. Ballarini, F. Mangione, G. Lerario, D. Sanvitto, and G. Gigli, ACS Photonics **1**, 1042 (2014).
[19]A. Cacciola, O. D. Stefano, R. Stassi, R. Saija, and S. Savasta, ACS Nano **8**, 11483 (2014).
[20]A. Kumar, T. Low, K. H. Fung, P. Avouris, and N. X. Fang, Nano Lett. **15**, 3172 (2015).
[21]J. Kasprzak, M. Richard, S. Kundermann, A. Baas, P. Jeambrun, J. M. J. Keeling, F. M. Marchetti, M. H. Szymanska, R. André, J. L. Staehli, V. Savona, P. B. Littlewood, B. Deveaud, and L. S. Dang, Nature **443**, 409 (2006).
[22]J. D. Plumhof, T. Stöferle, L. Mai, U. Scherf, and R. F. Mahrt, Nat. Mater. **13**, 247 (2014).
[23]K. S. Daskalakis, S. A. Maier, R. Murray, and S. Kéna-Cohen, Nat. Mater. **13**, 271 (2014).
[24]A. Amo, D. Sanvitto, F. P. Laussy, D. Ballarini, E. del Valle, M. D. Martin, A. Lemaître, J. Bloch, D. N. Krizhanovskii, M. S. Skolnick, C. Tejedor, and L. Viña, Nature **457**, 291 (2009).
[25]A. Amo, J. Lefrère, S. Pigeon, C. Adrados, C. Ciuti, I. Carusotto, R. Houdré, E. Giacobino, and A. Bramati, Nat. Phys. **5**, 805–810 (2009).
[26]I. Carusotto and C. Ciuti, Rev. Mod. Phys. **85**, 299 (2013).
[27]L. S. Dang, D. Heger, R. André, F. Bœuf, and R. Romestain, Phys. Rev. Lett. **81**, 3920 (1998).
[28]P. Senellart and J. Bloch, Phys. Rev. Lett. **82**, 1233 (1999).
[29]S. Christopoulos, G. B. H. Hoügersthal, A. J. D. Grundy, P. G. Lagoudakis, A. V. Kavokin, J. J. Baumberg, G. Christmann, R. Butté, E. Feltin, J. F. Carlin, and N. Grandjean, Phys. Rev. Lett. **98**, 126405 (2007).
[30]D. Ballarini, M. D. Giorgi, E. Cancellieri, R. Houdré, E. Giacobino, R. Cingolani, A. Bramati, G. Gigli, and D. Sanvitto, Nat. Commun. **4**, 1778 (2013).
[31]C. Monroe, Nature **416**, 238 (2002).
[32]Z. H. Tang, R. W. Peng, Z. Wang, X. Wu, Y. J. Bao, Q. J. Wang, Z. J. Zhang, W. H. Sun, and M. Wang, Phys. Rev. B **76**, 195405 (2007).
[33]K. Zhang, C. Wang, L. Qin, R. W. Peng, D. H. Xu, X. Xiong, and M. Wang, Opt. Lett. **39**, 3539 (2014).
[34]D. M. Coles, N. Somaschi, P. Michetti, C. Clark, P. G. Lagoudakis, P. G. Savvidis, and D. G. Lidzey, Nat. Mater. **13**, 712 (2014).
[35]D. M. Coles and D. G. Lidzey, Appl. Phys. Lett. **104**, 191108 (2014).
[36]S. Balci and C. Kocabas, Opt. Lett. **40**, 3424 (2015).
[37]W. L. Barnes, A. Dereux, and T. W. Ebbesen, Nature **424**, 824 (2003).
[38]J. B. Pendry, L. Martın-Moreno, and F. J. Garcia-Vidal, Science **305**, 847 (2004).
[39]R. H. Fan, J. Li, R. W. Peng, X. R. Huang, D. X. Qi, D. H. Xu, X. P. Ren, and M. Wang, Appl. Phys. Lett. **102**, 171904 (2013).
[40]A. Vázquez-Guardado, A. Safaei, S. Modak, D. Franklin, and D. Chanda, Phys. Rev. Lett. **113**, 263902 (2014).